This article has been accepted for publication in a future issue of this journal, but has not been fully edited. Content may change prior to final publication. Citation information: DOI 10.1109/JLT.2017.2715336, Journal of Lightwave Technology

Comb-Assisted Cyclostationary Analysis of Wideband RF Signals

Daniel J. Esman, Vahid Ataie, Bill P.-P. Kuo, Eduardo Temprana, Nikola Alic, and Stojan Radic

***Abstract*— Signals arising in nearly all disciplines, including telecommunications, mechanics, biology, astronomy, and nature are generally modulated, carrying corresponding signatures in both the temporal and spectral domain. This fact was long recognized by cyclostationary and cumulant analysis, providing qualitatively better means to separate stochastic from deterministically modulated radiation. In contrast to simple spectral analysis, the cyclostationary technique provides a high level of spectral discrimination, allowing for considerable signal selectivity even in the presence of high levels of background noise and interference. When performed with sufficient resolution, cyclostationary analysis also provides the ability for signal analysis and classification. Unfortunately, these advantages come at a cost of large computational complexity posing fundamental detection challenges. In the case of modern ultrawideband signals, the requirements for persistent cyclostationary analysis are considerably beyond the processing complexity of conventional electronics. Recognizing this limit, we report a new photonically-assisted cyclostationary analyzer that eliminates the need for high-bandwidth digitization and real-time Fourier processors. The new receiver relies on mutually coherent frequency combs used to generate a Fourier representation of the received signal in a computation-free manner. With the advent of practical, cavity-free optical frequency combs, the complexity for cyclostationary analysis can be greatly reduced, paving a path towards persistent wideband cyclostationary analysis in an ultrawideband operating regime.**

***Index Terms*: Cyclostationary Receiver, Spectral Analysis, Frequency Combs, Noise Discrimination.**

I. INTRODUCTION

SIGNAL detection, classification and interpretation (DCI) across the entire radio-frequency (RF) spectrum poses both fundamental and technological challenges. While high resolution, high-sensitivity DCI can be performed in a local (narrow-band) manner, such spectral analysis is generally not viable over the contiguous RF range (3kHz-300GHz) hosting modern communication and sensing applications. The wideband challenge is further compounded by the fact that emission may contain bursty, frequency-hopping or spectrally-spread signals that eliminate, even in principle, conventional averaging or fixed-band filtering techniques. As an example, a modern ultrawideband (UWB) emission is modulated at rates that exceed GHz, has a carrier that can be varied over 10s of GHz and exists as a short duration burst. Worse, such a signal is often buried under intense RF traffic or is deliberately jammed by band-matched waveforms. Similar to man-made emission, natural radiation can resemble UWB signaling in terms of bandwidth, spectral content and its transience. In both cases, the DCI challenge is similar: a faint signal must be detected across a wide spectral range, extracted from noise, classified and ultimately reconstructed (demodulated).

The wideband challenge can be addressed by devising a backplane of either a global (full-bandwidth), or multiple, spectrally-localized receivers. The former approach is clearly unrealistic for a band of interest that approaches 100 GHz or more. In contrast, the latter strategy requires a band-tunable (scanning) or spectrally-segmented (banded) receiver architecture. A scanning approach not only does not stare at the entire band in real time but also incorporates a tunable filter that inevitably imposes a performance limit: an increase in scanning rate is paid in terms of spectral resolution. In contrast, spectral segmentation (channelization) can circumvent this limitation, albeit at the expense of increased complexity: each sub-band must be served by a separate processing device and, in most cases, these need to be synchronized across the entire backplane. A conventional RF channelizer [1] represents an example of a widely used spectrally-segmented DCI architecture. To be effective, a channelizer must combine low loss, high inter-band isolation and possess a rapid roll-off rate [1] to avoid spectral information loss. Unlike an all-electronics channelizer, a photonic-assisted topology can address all these requirements while possessing THz-wide response – sufficiently wide to accommodate multiples of the contiguous RF spectral range. Notably, photonic-assisted channelizer architectures have been developed and used to demonstrate low-latency frequency monitoring and spectral analysis [2], [3], [4].

While near-ideal channelization is desirable, this is not sufficient for detection of UWB signals accompanied by natural or artificial interference. To detect a wideband signal in a contested electromagnetic (EM) environment, it is necessary to discriminate a deterministic waveform from stochastic or quasi-stochastic radiation. A practical solution for noise discrimination was provided early [5] and embedded in modern cyclostationary (CS) and cumulant receivers [6], [7]. Intuitively elegant, CS analysis separates signal and stochastic interference using a simple criterion: a modulated waveform is periodically correlated, while noise remains

This work was supported in part by the Defense Advanced Research Agency (DARPA).

D.J. Esman, V. Ataie, B.P-P Kuo, E. Temprana and S. Radic are with the department of Electrical and Computer Engineering, University of California San Diego, La Jolla, Ca 92039 USA (email: desman@ucsd.edu; vataie@ucsd.edu; p2kuo@ucsd.edu; sradic@ucsd.edu).

N. Alic is with the California Institute for Telecommunications and Information Technologies, University of California San Diego, La Jolla, CA 92093 USA (email: nalic@ucsd.edu).

inherently uncorrelated. Since its introduction, the CS approach, and its generalization (cumulant analysis), has been adopted in a broad range of applications, including communications [7], atmospheric sciences [8], [9], [10], machinery [11], biology [12], and econometrics [13].

Unfortunately, the practical advantages of a CS analyzer fade when the signal bandwidth exceeds the speed of a viable electronic processor. A modern cyclostationary receiver relies on a high-precision digitizer and real-time Fourier transformer in order to calculate the spectral correlation function (SCF) [6]. To analyze a wide RF range, a CS analyzer must possess an analog-to-digital converter (ADC) that matches the received signal bandwidth. In practice, this means that the detection of UWB signals [14] emitted within a wide RF range (10s of GHz) also imposes a fundamental ADC resolution limit [15], [16]. At the same time, the real-time Fourier mapping of the received signal poses a more difficult technology challenge. While conventional (electronic) processors rely on a fast Fourier transform (FFT) algorithm [17], its complexity still prevents real-time processing at UWB rates. As a result, the combined (ADC/FFT) processing barrier imposes a strict limit on the cyclostationary receiver performance. While real-time CS analyzers can be operated over sub-GHz bandwidths [18], [19], none, to the best of our knowledge, has approached a sizeable fraction of the contiguous RF range.

Recognizing these limits, we introduce and demonstrate a new class of CS analyzer that completely eliminates a high-bandwidth ADC, and, more importantly, dispenses with a need for computational Fourier mapping of the received emission. To accomplish these functions, the new architecture incorporates mutually coherent frequency combs to decimate the emission bandwidth and obtain the discrete Fourier transform (DFT) in the physical domain. Consequently, we describe the construction and operating performance of the new CS analyzer operating over 20 GHz of aggregate bandwidth. A composite RF signal, consisting of QPSK, 8-PSK and BPSK waveforms centered at 2.5, 6 and 9 GHz carriers, respectively, was detected and classified under varied noise-loading conditions. The detection performance of the cyclostationary receiver was compared to simulated results.

The remainder of this paper is organized as follows: we discuss fundamental and practical limits of a conventional (electronic) CS analyzer in Section II, the operational principles of the proposed cyclostationary receiver are introduced in Section III; and the experimental architecture is described in Section IV. The experimental results and performance analysis are detailed in Section V, with discussion and concluding remarks closing the Section VI.

II. Conventional CS Architecture Limits

A CS receiver separates signal from noise (interference) by taking advantage of the cyclical nature of any modulation format. To illustrate this principle, we assume that the received radiation $r(t)$ can be written as a summation of modulated signal $s(t)$ and noise $n(t)$ contributions:

$$r(t) = s(t) + n(t) = \sum_m \prod (mT)B(t - mT) + n(t)$$

where a cycle modulation waveform is denoted by Π, with modulation cycle duration T and encoded data by B. While the modulated signal portion of the received field is not strictly periodic, its autocorrelation $R_r(t,\tau) = \left\langle r(t)\, r(t-\tau)^* \right\rangle$ is [5]:

$$R_r(t,\tau) = R_r(t+T,\tau).$$

Since the autocorrelation is temporally periodic, one can define the Fourier transform [5] using the auxiliary variable α:

$$R_r^{\alpha}(\tau) = \lim_{T\to\infty} \frac{1}{T} \int_T r\left(t + \frac{\tau}{2}\right) r\left(t - \frac{\tau}{2}\right)^* e^{-j2\pi\alpha t} dt .$$

Finally, by mapping the last expression to the Fourier domain:

$$S_r^{\alpha}(f) = \int_{-\infty}^{\infty} R_r^{\alpha}(\tau) e^{-j2\pi f\tau} d\tau ,$$

one has defined the well-known spectral correlation function (SCF) that represents a complex transform in 2-dimensional α-f space. A typical SCF function that operates on multiple signals is illustrated in Fig. 1, in case when accompanying noise is near-achromatic. The SCF plot in Fig.1 is readily used to intuitively understand the power of cyclostationary analysis. In the case when the received waveform is white noise, its spectral components will exhibit no correlation, requiring that SCF function vanishes for $\alpha \neq 0$. This is apparent in Fig. 1, where the plotted power density corresponding to noise contribution is almost entirely confined at $\alpha = 0$. Conversely, signal features are prominent at non-zero α locations (α-f plane), providing for effective discrimination means between signal and noise. Unfortunately, to obtain SCF mapping shown in Fig. 1, a CS analyzer must use a chain of high-complexity processing blocks, as shown in Fig. 2. The received signal is first digitized (ADC) and then subsequently mapped to the Fourier domain (FFT). After the spectral representation is obtained, spectral correlation is computed in order to generate the two-dimensional SCF representation, discriminating the noise. A wideband ADC poses the first processing challenge that can be quantified in terms of precision, operating bandwidth and dissipation. While an ADC capable of contiguous RF range is unlikely to be constructed in the near future [16], circuits operating beyond 20 GHz have been reported [16]. If we assume that an RF bandwidth of

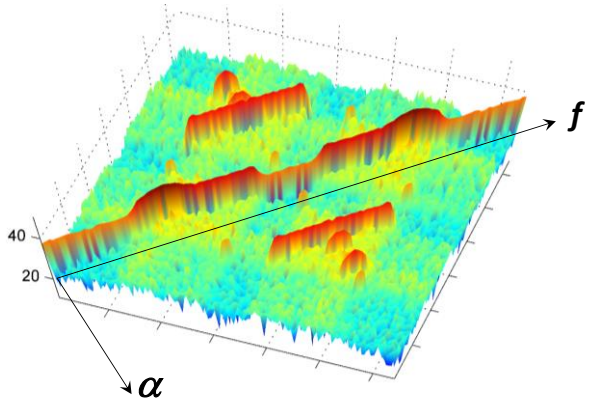

Fig. 1. SCF ($S_r^{\alpha}(f)$) mapped in two-dimensional (α-f) space.

This article has been accepted for publication in a future issue of this journal, but has not been fully edited. Content may change prior to final publication. Citation information: DOI 10.1109/JLT.2017.2715336, Journal of Lightwave Technology

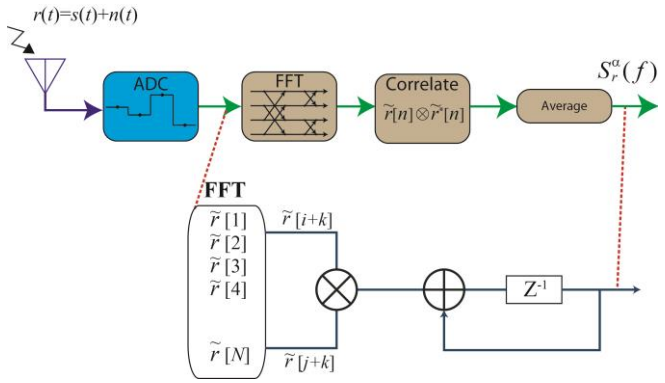

Fig. 2. Conventional CS Receiver Architecture.

100 GHz can be addressed by a combination of multiple ADC stages, such a compound digitizer would still dissipate nearly 100 Watts. Even if this were acceptable in a select set of CS applications, the effective number of bits (ENOB) of such a digitizer will strictly limit its utility. While recently reported ADC demonstrations were performed at rates above 20 GHz these still possess ENOB ~ 7 [16]. Limited digitizer precision is critical since it precludes, even in principle, classification of a high-complexity or closely spaced signals.

While an ADC imposed limit might appear formidable, it is both the computational complexity and precision of the FFT processor as well as the computation of the correlation over large bandwidths that sets the fundamental limit on any CS construction. While much work has been done to reduce the computational complexity of the correlation computation [20], [21], [22], they still rest on a high precision, fast FFT. To understand this important notion, consider a case when one must detect and classify a spread-spectrum signal in presence of noise or interference, as illustrated in Fig. 3.

A spread-spectrum channel carrying information $x[k]$ (at k^{th} bit of the transmitted stream) is modulated using a codeword $c[k]$ at a much higher rate (chip-rate) [23]. To understand the FFT-imposed limit, consider having to identify two different users each using two distinct codewords. In the complex Fourier plane (Fig. 3b), with an increase in codeword length (N), the distance between the complex coefficients of the codeword in I-Q plane decreases. As an upperbound of the precision required to distinguish between two signals modulated by different codewords, it is necessary to resolve the two closest points between codewords in I-Q constellations, as shown in Fig. 3b (inset). This means that in this case, the FFT precision should be sufficient to resolve the smallest distance between two codeword points in the I-Q plane. Undeniably, this least upperbound on FFT precision will be much more stringent in a more practical situation. This can be understood in the case when signal time of arrival is unknown, yielding a complex rotation amongst each of the codewords in the complex Fourier plane. This in turn greatly reduces the distance between two coefficients, and hence, mandating a much higher FFT precision. While high precision is possible in conventional electronic FFT processors, operating at sub-GHz rates [17], this is not viable at rates of interest here (10s of GHz) that remain nearly two

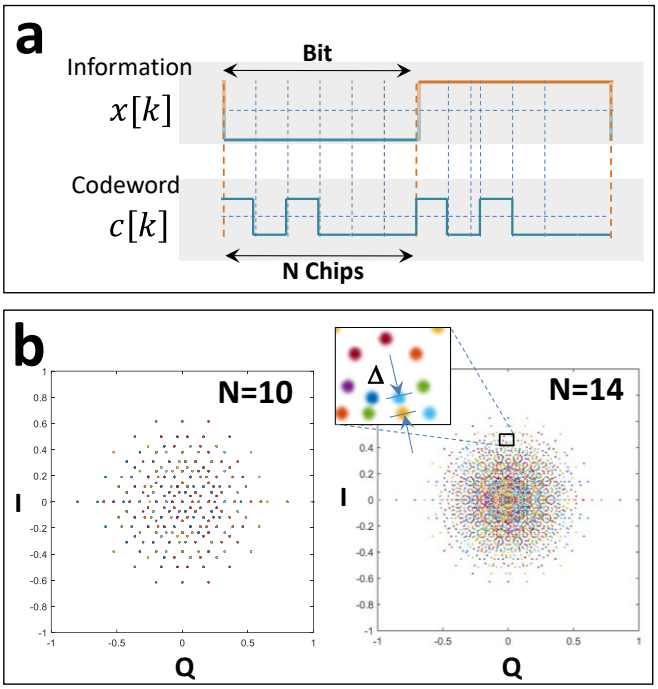

Fig. 3. Spread-Spectrum Signal representation in Fourier domain: all possible combinations of direct-sequence coding is plotted for codeword length N = 10 (bottom left) and N = 14 (bottom right).

orders of magnitude higher. The complexity-bandwidth FFT limit is deceptively similar to the familiar argument used in general-purpose processors, where one hopes to match any processing gain by decrease in feature size. Unfortunately, this cannot be made in case of FFT CMOS architecture that underpins nearly all CS processors. An FFT algorithm critically relies on multiplication and addition operations [17], with a multiplier CMOS cell dominating its dissipation [17]. In addition, any increase in FFT bit precision imposes a quadratic increase in gate count [24]. Even if one assumes that the gate increase can be accomplished with ideal gate-to-gate connectivity (i.e. zero-dissipation, at any operating rate), this effectively means that the FFT core precision still imposes at least quadratic dissipation law. In practical terms, a two-order increase in operating speed is likely to lead to unsurmountable connectivity loss and unsustainable heat dissipation [25].

Recognizing the fundamental limits imposed on both the ADC and FFT processing cores in a CS receiver, the new architecture eliminates both stages. Rather than digitizing a wideband signal and then computing its FFT in real time and at high precision, the received field is mapped to the Fourier domain in a computation-free manner, as shown in Fig. 4. The new CS analyzer front end uses two coherently coupled frequency combs; the first one serves to replicate the received radiation, while the second one provides an array of local oscillator (LO) tones, frequency-matched to each generated signal copy. The two combs possess a different frequency pitch, with the difference (δf) defining the frequency resolution of the physical Fourier preprocessor, and not necessarily that of the composite CS analyzer. In contrast to incoherent spectral analyzers, the received RF signal is used to

This article has been accepted for publication in a future issue of this journal, but has not been fully edited. Content may change prior to final publication. Citation information: DOI 10.1109/JLT.2017.2715336, Journal of Lightwave Technology

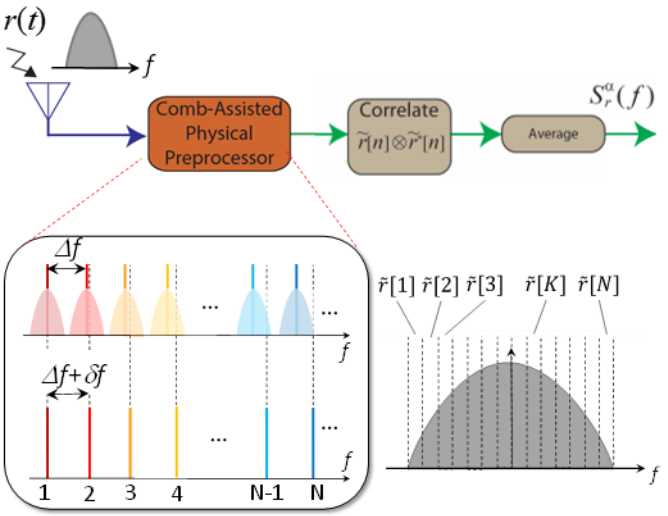

Fig. 4. Comb-Assisted CS analyzer architecture: mutually coherent combs with precisely controlled frequency pitch eliminate ADC-FFT processing chain. Local oscillator comb probes signal at different frequencies, resulting in coherent band segmentation (right bottom).

modulate a frequency comb and create N spectral replicas, preserving both phase and amplitude. These copies are combined with a coherent LO comb, allowing each pair to be received by a low-bandwidth (δf) detector array. As a result, the backplane array outputs the discrete Fourier transform (DFT) of the received field (denoted as $\tilde{r}[k], k = 1, N$ in Fig. 4). The tone-count of frequency combs directly controls the speed of the fastest electronic component in the processing chain. As an illustration, 100 GHz CS analysis performed by combs with moderate (1500) tone count, dictates a 60 MHz-rate electronic backplane. Remarkably, a high-precision (ENOB > 10) ADC operating at this rate consumes approximately 0.2 mW [16], in sharp contrast to a full-band (100 GHz) device. More importantly, an FFT processor is entirely eliminated, thus resolving one of the most important technological limitations of a wideband CS analyzer.

III. Implementation

The use of near-noiseless and distortionless signal replication and subsequent frequency decomposition are unique attributes of the new cyclostationary receiver, as illustrated in Fig. 4. First, the received electrical signal is replicated onto a coarsely spaced (ΔF) optical frequency grid. This is achieved by modulating the received electrical signal onto an optical frequency comb (signal frequency comb). A second, Vernier comb, referenced to the signal comb with a pitch offset δf from ΔF is generated. The two combs were frequency locked by sharing the same master optical oscillator as a seed, and frequency-locked RF synthesizers. Each comb is then sent to unique arrayed waveguide gratings (AWG), which splits each optical mode into individual fibers. Finally, each of the overlapping comb tones is sent to a low speed coherent receiver. The selected Vernier comb line acts as a frequency-referenced local oscillator for a specific sub-band of the electrical signal, effectively down-converting the designated frequency band to baseband. The down-converted electrical frequency components are then captured by the low

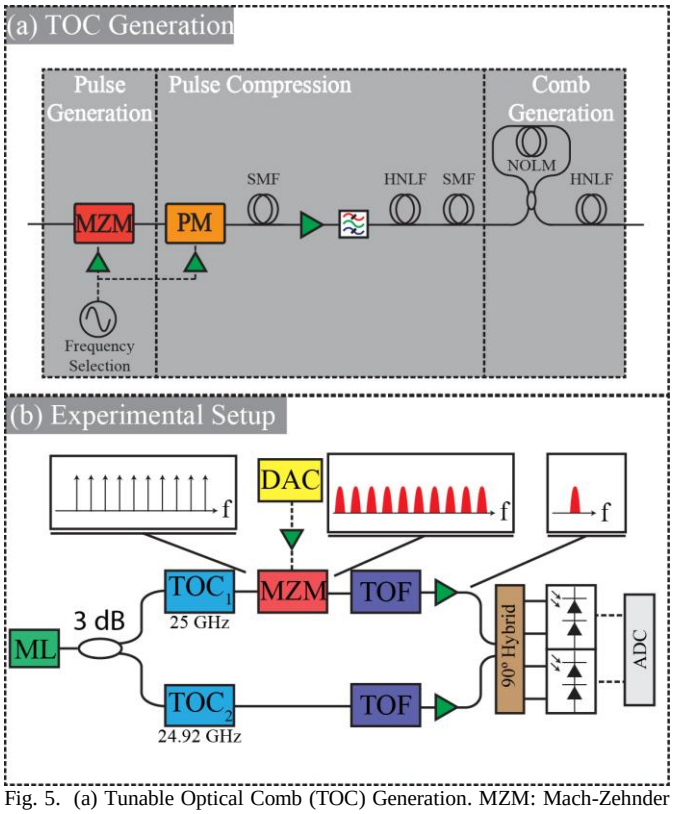

Fig. 5. (a) Tunable Optical Comb (TOC) Generation. MZM: Mach-Zehnder modulator, PM: Phase modulator, SMF: Single mode fiber, HNLF: Highly nonlinear fiber, NOLM: Nonlinear optical loop mirror. (b) Experimental Setup. ML: Master laser, DAC: Digital-to-analog converter, TOF: Tunable optical filter, ADC: Analog-to-digital converter.

speed receiver. Consequently, the input electrical spectrum is completely decimated, akin to a lossless, but coherent channelization. We note that the architecture, while resembling the conventional channelizer, does not have any physical filters, and, more importantly, does not operate on signal spectral power, but on the entire received field. In this respect, the preprocessor is more similar to the vector analyzer, except that it can operate in real time, without any blind intervals.

The resolution at which the frequency decomposition can be achieved is directly proportional to the number of optical frequency comb modes that are utilized. In the simplest implementation, high resolution is achieved by incorporating maximal number of optical frequency modes. Although it is possible to drastically reduce the number of comb tones and corresponding subrate detector elements while maintaining the same resolution, this subject will be addressed in a subsequent report.

Several techniques have been used to generate optical frequency combs, including the widely used mode-locked lasers [19], micro-resonators [26], and cascaded E/O modulator derived combs [27], [28]. In this work, we rely on the parametric comb generation technique, previously shown to successfully integrate frequency reconfigurability (both center frequency and pitch), ultrahigh count (thousands of lines), and high spectral purity (high OSNR) at the same time [29].

A literal implementation of a comb-assisted CS architecture

calls for each signal-LO pair created by the modes from the signal and reference comb to be routed by an arrayed waveguide grating (AWG) and subsequently to a bank of low speed coherent detectors. Each detector would yield a single spectral decomposition element of the received electrical field. However, to demonstrate the scalability of this architecture without fully populating the low speed detector backplane, the performance of the receiver can be rigorously characterized with a single low speed receiver. The use of a single receiver in capturing multiple channels is a well-established technique in WDM transmission, where the performance of each channel is measured sequentially at the end of the link. Applying the equivalent to WDM sequential approach, a single, low speed coherent receiver is used to successively capture each of the signal and LO modes individually. For an accurate emulation of the full-scale implementation, the received electrical noise has to be repeated during each of the successive captures. Consequently, the noise was generated in the digital domain and added to the electrical signal before being converted to the analog domain with a digital to analog converter (DAC). However, this technique, while relieving the construction from assembling the full detector array, also imposes a unique challenge in the characterization of the receiver. Firstly, the noise statistics and bandwidth will be set by the resolution and bandwidth of the DAC, respectively. Consequently, it is necessary to use a DAC with a high bandwidth and sufficient effective number of bits (ENOB) to synthesize adequate noise statistics during the characterization of the CS receiver. Secondly, the sequential signal capture imposes a unique stability challenge during the characterization of the receiver: the entire receiver, and in particular, the two optical frequency combs must remain stable during the entire capture time. To appreciate this requirement, we note that a typical signal of interest lasts nanoseconds; in contrast, sequential CS capture can last hours. This limitation is substantially mitigated by the fact that frequency-referenced combs have been derived from a single (fixed) frequency source and that no stabilized optical cavity was used anywhere in the testbed. As a result, all results reported here were easily replicable, both over short scale (minutes) and long scale (hours). This feature has particular importance in case when the entire CS analyzer must operate in harsh (airborne or spaceborne) environment subject to stress and temperature variation. Intuitively, the observed stability is rooted to a simple fact that two frequency combs, while drifting in frequency over time (master oscillator was not locked), *they do so together, strictly maintaining their relative frequency/phase relations*. Although this approach utilizes sequential capturing of each DFT coefficient which introduces latency to the capture time, a full detector backplane would remove this latency allowing for real time operation. However, utilizing a full detector backplane may not be viable when the detector count is greatly increased (e.g. for enhanced resolution). In such case, the total number of detectors can significantly be decreased by increasing the bandwidth of each detector, allowing for multiple DFT coefficients to be captured by each detector, greatly reducing the total required detector count. While this method will reduce the total number of required detectors, it does require additional computational complexity in the digital domain to extract each of the DFT coefficients. The ideal number of detectors, and the bandwidth of each, will be dependent on the implementation requirements.

Finally, after spectral decomposition, the SCF is estimated by taking the vector outer product of the physically generated DFT components with the conjugate of itself. The entire process is repeated and averaged over time, varied with different signal stimuli.

IV. Experiment

The experimental comb generation technique is depicted in Fig. 5(a). A single high quality master laser (ML) oscillator operating at 1559.2 nm was used as a seed to both optical frequency combs. The ML was split into two paths with a 3-dB coupler. The signal path was defined by a 25 GHz-pitched optical frequency comb. To generate a high SNR optical frequency comb, broadband optical pulses were first synthesized using the master oscillator as a carrier and a conventional Mach-Zehnder modulator (MZM) driven with an RF 25 GHz tone. The pulses were subsequently tailored in the first compression stage, first by inducing a chirp with a phase modulator (PM), driven with identical RF 25 GHz tone, and subsequently compressed within a section of single mode fiber (SMF). After amplification and filtering, the optical pulses were then shortened in a second compression stage. The chirp in the second compression stage was generated by self-phase modulation (SPM) in a highly nonlinear fiber (HNLF), with subsequent compression achieved in a 2nd section of SMF. Next, the pulses were precisely shaped in a nonlinear optical loop mirror (NOLM) architecture. Finally, the high peak power, pedestal-free pulses were launched into the final HNLF stage, where cascaded four wave mixing (FWM) was used to generate a wideband optical frequency comb with 25 GHz spacing. The generated comb is shown in Fig. 6 and consisted of over 400 optical modes, with minimum of 43 dB $SNR_{0.1nm}$. We note that OSNR was limited by the measurement device sensitivity; true OSNR was likely higher. A similar technique was used to generate a second (reference) comb, using a 24.92 GHz RF seed to generate the desired δf = 80 MHz pitch difference between the two combs.

The experimental CS setup is shown in Fig. 5(b). After the comb generation, the signal comb was modulated by the electrical input test signal. This effectively replicated the incoming electrical signal onto each of the 250 optical

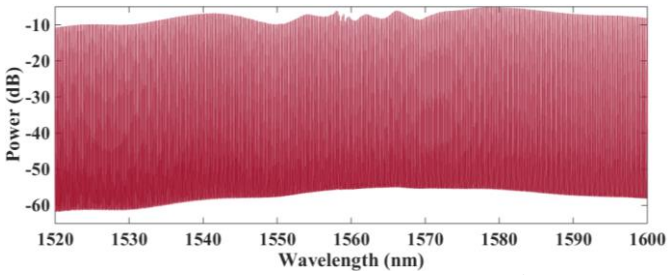

Fig. 6. Constructed 25 GHz pitched tunable optical frequency comb. Measurement performed in 0.02 nm resolution bandwidth.

This article has been accepted for publication in a future issue of this journal, but has not been fully edited. Content may change prior to final publication. Citation information: DOI 10.1109/JLT.2017.2715336, Journal of Lightwave Technology

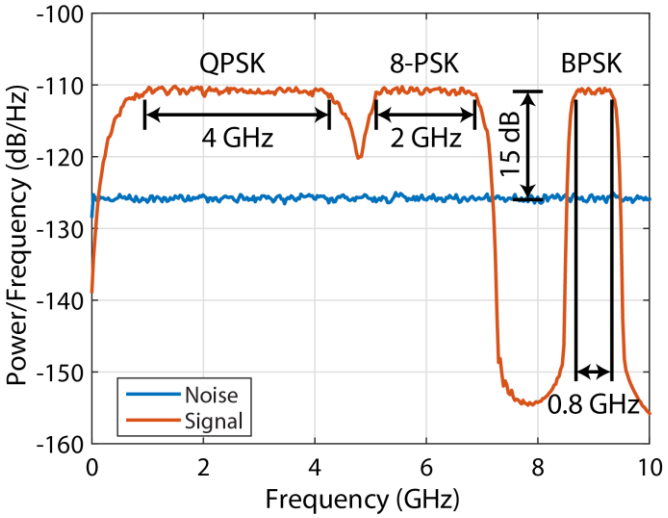

Fig. 7. Electrical 15 dB SNR input Spectrum consisting of 4 GHz QPSK signal at 2.5 GHz carrier frequency, 2 GHz 8-PSK signal at 6 GHz carrier frequency, and 800 MHz BPSK signal at 9 GHz carrier frequency.

carriers. Next, both optical frequency combs were sent to two separate programmable optical filters. The filters were used to emulate an AWG, whereby each optical mode was sequentially filtered out individually. The pair of overlapping signal and reference comb tones were then amplified with either C- or L- band erbium doped fiber amplifiers (EDFA) before being sent to a 40 GHz hybrid detector. The output was then sent to an electrical ADC whose bandwidth and sampling rate were set to 80 MHz. After the capture, the programmable optical filter was then tuned to select the next pair of overlapping optical tones. Finally, post-processing was applied after all 250 optical modes were captured by the ADC.

The electrical test signal was generated using a 60 GS/s DAC. The DAC was used to synthesize both the signal and noise. The signal consisted of 4 GHz quadrature phase shift keyed (QPSK) raised cosine shaped data with 0.25 rolloff factor and upconverted to 2.5 GHz carrier. Additionally, a 2 GHz wide, 8-PSK raised cosine shaped signal and an 800 MHz binary phase shift keyed (BPSK) raised cosine shaped signal were also generated and upconverted to 6 GHz, and 9 GHz, respectively. The three signals were generated without any chirp and simultaneously stimulated with noise to achieve an in-band SNR of 15 dB, 10 dB, and 5 dB. The digital signal stimuli and noise spectrum are illustrated in Fig. 7. The generated electrical signal was then amplified and used to modulate the 25 GHz signal comb utilizing a null-biased MZM.

The DSP that was applied at the receiver consisted of channel timing and phase alignment, filtering and subsequent downsampling to 80 MHz in order to estimate the 250 DFT coefficients over a 12.5 ns window. Phase alignment was used to remove any random phase fluctuations associated with path length variations in addition to any dispersion or chirp introduced between the two frequency combs. The SCF function was then calculated by taking the vector outer product of the estimated DFT coefficients with the conjugate of itself. The process was repeated and averaged over an approximately 4.2 μs time window, corresponding to 333 total

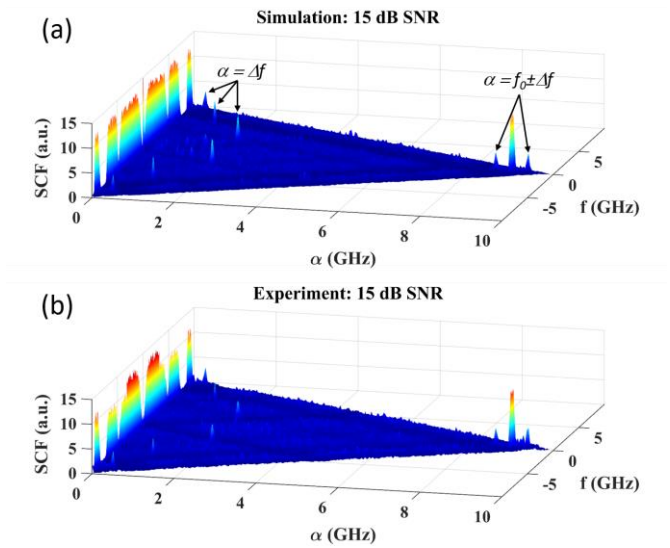

Fig. 8. (a) Simulated SCF results with 250 point DFT and 15 dB SNR. BPSK features at Δf and $f_0 \pm \Delta f$ are distinguished. (b) Measured experimental SCF results with 250 point DFT and 15 dB SNR.

averages. The number of averages was limited by the total memory depth of the DAC utilized.

V. Experimental Results

To test the performance of the new analyzer architecture, the SCF was calculated in two ways. First, the SCF was simulated in the digital domain, computing the 250 point DFT, and subsequently yielding the SCF estimation. The estimation was reached by averaging 333 realizations of the SCF of the input electrical signal. Secondly, the electrical signal was then sent into the cyclostationary receiver whereby the 250 DFT coefficients were estimated using the new architecture, and the SCF estimation was then reached by averaging 333 realizations of the SCF. The estimated SCF was then

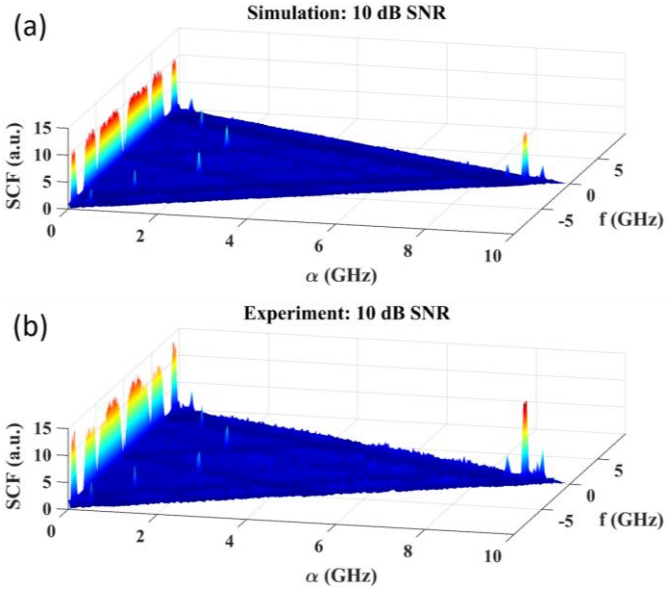

Fig. 9. (a) Simulated SCF results with 250 point DFT and 10 dB SNR. (b) Measured experimental SCF results with 250 point DFT and 10 dB SNR.

This article has been accepted for publication in a future issue of this journal, but has not been fully edited. Content may change prior to final publication. Citation information: DOI 10.1109/JLT.2017.2715336, Journal of Lightwave Technology

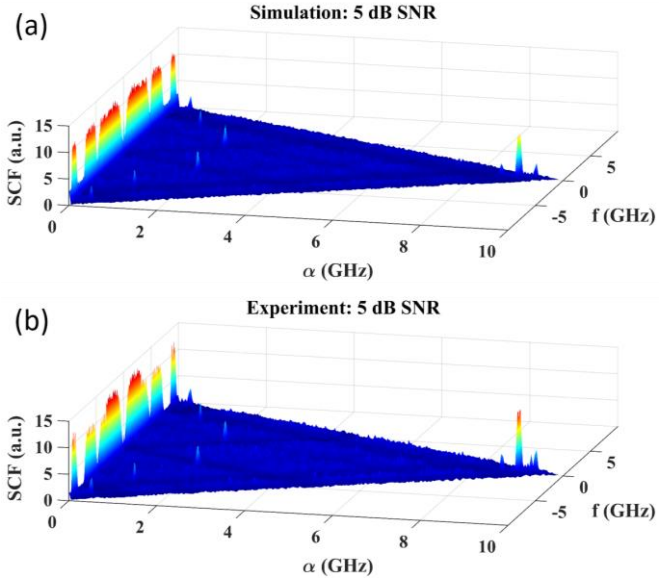

Fig. 10. (a) Simulated SCF results with 250 point DFT and 5 dB SNR. (b) Measured experimental SCF results with 250 point DFT and 5 dB SNR.

compared with the simulated SCF. The simulated SCF and experimental SCF for an input SNR of 15 dB is shown in Fig. 8(a) and (b), respectively. In both plots, distinct features appear in the α-f domain, as expected from the QPSK, 8-PSK, and BPSK modulated signals. We note that simulated and experimental results match extremely well, both with respect to feature extraction and overall magnitudes. For a BPSK signal, strong spectral correlation exists at the carrier frequency rate $\alpha = f_0$, at the modulation rates $\alpha = \pm\Delta f$, and at $\alpha = f_0 \pm \Delta f$ [30], as indicated in Fig. 8(a) and (b). For QPSK and 8-PSK, strong spectral correlation does not exist at the carrier frequency, due to the modulation being balanced between in-phase and quadrature components [30]. In both the simulated and experimental data, strong spectral correlation for QPSK and 8-PSK is indeed only observed at the keying rates $\alpha = \pm\Delta f$, as depicted in Fig. 8(a) and (b).

The proposed system was also characterized in lower SNR regimes. This was achieved by increasing the noise power relative to the signal in the digital domain before uploading the data to the DAC. For an input SNR of 10 dB, the simulated and experimentally estimated SCF are plotted in Fig. 9(a) and (b), respectively. Even at this lower input SNR, both the simulated and the computationally efficient experimental SCF exhibit strong features in the cyclic domain. Also, even in the lower SNR regime, the experimental data matches closely with the simulated data, with features that match well with the analytic expectation.

Remarkably, the system SNR was lowered to 5 dB, maintaining the similar agreement between the simulation and experiment. Even in this low SNR regime, the simulated SCF matched closely with the low complexity experimental SCF, as shown in Fig. 10(a) and (b). In both cases, strong spectral correlation peaks are observed in the cyclic domain that match the theoretically predicted features. Specifically, for an environment with large interfering noise, where the signal is only 5 dB above the noise, high confidence signal detection

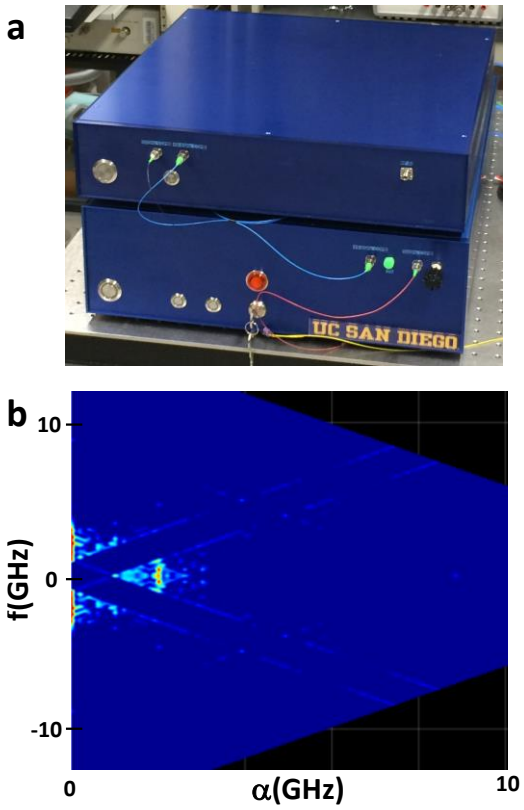

Fig. 11. (a) Packaged CS Analyzer consisting of two mutually coherent optical frequency combs (lower box), and receiver backplane for electrical input modulation and CS analysis (upper box). (b) SCF output generated by 2 GHz BPSK signal stimulus at a 2 GHz carrier frequency.

and classification can be achieved with low computational complexity utilizing the new experimental architecture.

Finally, to demonstrate the practical utility of the new approach, a CS receiver was designed, constructed and packaged within a standard telecommunication module, as shown in Fig. 11(a). This portable system operated over 38 GHz bandwidth with 200 MHz spectral resolution. To validate the receiver performance, a 2 GHz BPSK signal up-converted to 2 GHz carrier frequency was used as a stimulus to the system. The output of the system which calculates the SCF function of the input is plotted in Fig. 11(b).

VI. Conclusion

We have designed, constructed and tested the first ultrawideband cyclostationary receiver that eliminates the need for full-band digitization and real-time Fourier computation. The low complexity of the new wideband receiver was made possible by generating a Fourier representation in the physical domain. The received field was decimated in the spectral domain using tunable, coherently coupled frequency combs that were derived from a single master oscillator. The new receiver was used to generate the SCF of multiple RF signal stimuli, and under varied SNR conditions. While this demonstration used only 250 comb tones to demonstrate the feasibility of computation-free Fourier mapping in a CS receiver, we recognize that parametric combs operating with thousands of tones allow for

considerably higher performance, both with respect to spectral resolution and signal selectivity. We expect that the new architecture evolves into different topologies that will optimize between the need to fully populate the receiver backplane and a need for low-latency operation.

REFERENCES

[1] G. W. Anderson. D. C. Webb, A. E. Spezio, and J. N. Lee, "Advanced Channelization Technology for RF, Microwave, and Millimeterwave Applications," *Proc. IEEE*, vol. 79, no. 3, pp. 355-388, Mar. 1991.

[2] A. O.J. Wiberg, D. J. Esman, L. Liu, J. R. Adleman, S. Zlatanovic, V. Ataie, E. Myslivets, B. P. P. Kuo, N. Alic, E. W. Jacobs, and S. Radic, "Coherent filterless wideband microwave/millimeter-wave channelizer based on broadband parametric mixers," *J. Lightw. Technol.*, vol. 32, no. 20, pp. 3609-3616, Oct. 2014.

[3] W. Wang, R. L. Davis, T. J. Jung, R. Lodenkamper, L. J. Lembo, J. C. Brock, and M. C. Wu, "Characterization of a coherent optical RF channelizer based on a diffraction grating," IEEE Trans. Microw. Theory Tech., vol. 49, no. 10, pp. 1996–2001, Oct. 2001.

[4] X. Xie, Y. Dai, K. Xu, J. Niu, R. Wang, L. Yan, and J. Lin, "Broadband photonic RF channelization based on coherent optical frequency combs and I/Q demodulators," IEEE Photon. J., vol. 4, no. 4, pp. 1196–1202, Aug. 2012.

[5] H. L. Hurd, "An investigation of periodically correlated stochastic processes", Ph.D. Dissertation, Duke University, Durham, NC, 1969.

[6] W.A. Gardner, "Representation and estimation of cyclostationary processes", Ph.D. Dissertation, Department of Electrical and Computer Engineering, University of Massachusetts, reprinted as Signal and Image Processing Lab Technical Report No. SIPL-82-1, Department of Electrical and Computer Engineering, University of California, Davis, CA, 95616, 1982, 1972.

[7] W. A. Gardner, A. Napolitano, L. Paura, "Cyclostationarity: Half a century of research," *Signal Proc.*, vol. 86, no. 4, pp. 639-697, Apr. 2006.

[8] Vecchia, A.V., "Periodic autoregressive-moving average (PARMA) modeling with applications to water resources," Water Res. Bull., vol. 21, no. 5, pp. 721–730, Oct. 1985.

[9] Y. P. Dragan, and I. Yavorskii, "The periodic correlation-random field as a model for bidimensional ocean waves," *Peredacha Informatsii*, vol. 51, pp. 15-25, 1982.

[10] P. Bloomfield, H. L. Hurd, and R. B. Lund, "Periodic Correlation in Stratospheric Ozone Data," *J. of Time Series Analysis*, vol. 15, no. 2, pp. 127-150, Mar. 1994.

[11] D. Konig, and J. R. Bohme, "Application of cyclostationary and time-frequency signal analysis to car engine diagnosis," *Acoustics, Speech, and Sig. Proc.*, vol. 4, pp. 149-152, Apr. 1994.

[12] T. Li, T. Qiu, and H. Tang, "Optimum heart sound signal selection based on the cyclostationary property," *Computers in Biology and Medicine*, vol. 43, pp. 607-612, Mar. 2013.

[13] E. Parzen, and M. Pagano, "An approach to modeling seasonally stationary time series," *J. of Econometrics*, vol. 9, pp. 137-153, 1979.

[14] J. Dederer, B. Schleicher, F. De Andrade Tabarani Santos, A. Trasser, and H. Schumacher, "FCC compliant 3.1–10.6 GHz UWB pulse radar system using correlation detection," *Proc. IEEE MTT-S Int. Microw. Symp. Dig. 2007*, pp. 1471–1474. 2007.

[15] R. H. Walden, "Analog-to-digital converter survey and analysis," IEEE J. Sel. Areas Commun., vol. 17, no. 4, pp. 539–550, Apr. 1999.

[16] B. Murmann. ADC performance survey 1997–2015. [Online]. Mar. 2015. Available: http://web.stanford.edu/~murmann/adcsurvey.html

[17] U. Meye-Baese, "Fourier Transforms," in *Digital Signal Processing with Field Programmable Gate Arrays*, 4th Ed. Springer, 2014, pp. 417-464.

[18] A. Tkachenko, D. Cabric, and R. W. Brodersen, "Cyclostationary Feature Detector Experiments using Reconfigurable BEE2," in *Proc. IEEE Int. Symposium on New Frontiers in Dynamic Spectrum Access Networks*, Dublin, Ireland, pp. 216-219, Apr. 2007.

[19] T. Yucek and H. Arslan, "A survey of spectrum sensing algorithms for cognitive radio applications," IEEE Commun. Surveys Tutorials, vol. 11, no. 1, pp. 116–130, First Quarter, 2009.S. T. Cundiff, and J. Ye, "Colloquium: Femtosecond optical frequency combs," *Rev. Mod. Phys.*, vol. 75, no. 1, pp. 325-342, Mar. 2003.

[20] R. S. Roberts, "Architectures for Digital Cyclic Spectral Analysis," PhD Dissertation, Department of Electrical Engineering and Computer Science, University of California, Davis, 1989.

[21] W. A. Gardner, "Cyclostationarity In Communications and Signal Processing," New York: IEEE Press, pp. 455-479, 1994.

[22] Kyouwoong Kim, Akbar, I. A., "Cyclostationary Approaches to Signal Detection and Classification in Cognitive Radio," DySPAN 2nd IEEE International Symposium on, pp. 212-215, 2007.

[23] A. J. Viterbi, " CDMA: principles of spread spectrum communication", Addison Wesley Logman Publishing Co., Inc. Redwood City (1995).

[24] G. W. Bewick, "Fast Multiplication: Algorithms and Implementation," Ph.D. Dissertation, Stanford University, Stanford, CA, 1994.

[25] E. Pop, S. Sinha, and K. E. Goodson, "Heat Generation and Transport in Nanometer-Scale Transistors," *Proc. IEEE*, vol. 94, no. 8, pp. 1587-1601, 2006.

[26] P. Del'Haye, O. Arcizet, A. Schliesser, R. Holzwarth, and T. J. Kippenberg, "Full stabilization of a microresonator-based optical frequency comb," *Phys. Rev. Lett.*, vol. 101, no. 5, Jul. 2008.

[27] R. Wu, V. R. Supradeepa, C. M. Long, D. E. Leaird, and A. M. Weiner, "Generation of very flat optical frequency combs from continuous-wave lasers using cascaded intensity and phase modulators driven by tailored radio frequency waveforms," *Opt. Lett.*, vol. 35, no. 19, pp. 3234-3236, Oct. 2010.

[28] L. P. Barry, R. Watts, E. Marthin, C. Browning, K. Merghem, C. Calò, A. Martinez, R. Rosales, and A. Ramdane "Characterization of optical frequency combs for OFDM based optical transmission systems," *Proc. Inter. Conf. on Fibre Opt. and Phot.*, Paper W2A.2 2012.

[29] V. Ataie, B. P.-P. Kuo, E. Myslivets, and S. Radic, "Generation of 1500-tone, 120nm-wide ultraflat frequency comb by single CW source," presented at the Opt. Fiber Commun. Conf., Anaheim, CA, USA, 2013, Paper PDP5C.1.

[30] W. A. Gardner, W. A. Brown III, C.-K. Chen, "Spectral Correlation of Modulated Signals: Part II-Digital Modulation," *IEEE Trans. On Comm.*, vol. 35, no. 6, Jun. 1987.